REALIZATION OF COMBINED DIAGNOSIS/TREATMENT SYSTEM BY ULTRASOUND STRAIN MEASUREMENT-BASED SHEAR MODULUS RECONSTRUCTION/IMAGING TECHNIQUE EXAMPLES WITH APPLICATION ON THE NEW TYPE INTERSTITIAL RF ELECTROMAGNETIC WAVE THERMAL THERAPY

C. Sumi, and R. Kojima
Department of Electrical and Electronics Engineering, Faculty of Science and Technology,
Sophia University, Tokyo 102-8554, JAPAN

Abstract - **For various soft tissues (e.g., breast, liver, etc.), we are developing the ultrasonic strain measurement-based shear modulus reconstruction/imaging technique. To clarify the limitation of this technique as the diagnostic tool, together with improving the technique we are collecting clinical shear modulus images. Furthermore, we are applying the technique as the monitoring technique for the effectiveness of chemical therapy (e.g., anticancer drug, ethanol) and thermal therapy (e.g., rf electromagnetic wave, HIFU, etc.). Here, we showed shear modulus images obtained in quasi-real time. Using the conventional Work Station, the quantitative images were obtained on ten seconds order. In particular, by exhibiting the superiority of shear modulus imaging compared with simultaneous B-mode imaging, we delineated the effectiveness of the technique as the clinical visualization technique for diagnosis and therapy. For instance, shear modulus value of *in vivo* human breast carcinoma was significantly high (typical value: 6.33 x 10^6 N/m^2). Shear modulus images were also obtained on *in vivo* human liver tissues. On the *in vitro* calf liver, shear modulus value of electromagnetic wave-induced thermal lesion became about five times higher after cooling down. We believe that this technique is solo currently available as diagnosis or monitoring tool, and yet in the near future this technique will allow the combined diagnosis/therapy systems for opening up a novel clinical style.**

Keywords – combined diagnosis/therapy system, cancer, ultrasonic strain measurement-based shear modulus reconstruction/imaging, differentiation, monitoring, effectiveness of treatment, chemical therapy, thermal therapy, interstitial RF electromagnetic wave thermal therapy, coagulation

I. INTRODUCTION

It is well known that the pathological stage of living human soft tissues highly correlates with the static mechanical properties. Then, as the diagnosis tool for various soft tissues (e.g., breast, liver, etc.), we are developing the ultrasonic strain measurement-based shear modulus reconstruction/imaging technique [1-6]. To clarify the limitation of this technique, together with improving the technique we are collecting clinical shear modulus images. Furthermore, As the static mechanical properties reversibly or irreversibly change by chemical therapy (e.g., anticancer drug, ethanol) and thermal therapy (e.g., rf electromagnetic wave, HIFU, LASER etc.) [7-12], we are applying the technique as the monitoring technique for the effectiveness of the therapy [13-15]. Here, we showed shear modulus images obtained in quasi-real time. Using the conventional Work Station (Compaq XP1000, Alpha 500 MHz), the quantitative images were obtained on ten seconds order. In particular, by exhibiting the superiority of the shear modulus imaging compared with the simultaneous B-mode imaging, we delineated the effectiveness of the technique as the quantitative visualization technique for diagnosis and therapy. Recently, to treat liver lesions several type interstitial RF electromagnetic wave thermal applicator systems are clinically used, in which the pair of needle-type electrodes and a plate electrode is employed. However, as we could confirm through *in vivo* human breast tissues that the technique has high potential as the practical tool for differentiating early stage malignancies [5], we in novel realized the thermal applicator using only needle electrodes. Since we'll also apply this diagnosis and therapy to *in vivo* deeply situated tissues, we conducted shear modulus imaging on *in vivo* liver as well as *in vivo* breast, after which, to verify the feasibility as the monitoring technique we performed heating/imaging on the fresh *in vitro* calf liver.

II. METHOD AND MATERIALS

A. Shear modulus reconstruction/imaging technique

In our imaging technique, the relative shear modulus distribution is reconstructed from ultrasonically measured strain tensor filed data with respect to reference shear moduli provided in properly realized local regions [1, 2].

Displacement vector field generated by spontaneous heart motion and/or externally applied pressures can be measured by

Report Documentation Page

Report Date	Report Type	Dates Covered (from... to)
25 Oct 2001	N/A	-

Title and Subtitle Realization of Combined Diagnosis/Treatment System By Ultrasound Strain Measurement-Based Shear Modulus Reconstruction/Imaging Technique Examples With Application on The New Type Interstitial RF Electromagnetic Wave Thermal Therapy	**Contract Number**
	Grant Number
	Program Element Number
Author(s)	**Project Number**
	Task Number
	Work Unit Number
Performing Organization Name(s) and Address(es) Department of Electrical and Electronics Engineering Faculty of Science and Technology Sophia University Tokyo 102-8554, Japan	**Performing Organization Report Number**
Sponsoring/Monitoring Agency Name(s) and Address(es) US Army Research, Development & Standardization Group (UK) PSC 803 Box 15 FPO AE 09499-1500	**Sponsor/Monitor's Acronym(s)**
	Sponsor/Monitor's Report Number(s)

Distribution/Availability Statement
Approved for public release, distribution unlimited

Supplementary Notes
Papers from 23rd Annual International Conference of the IEEE Engineering in Medicine and Biology Society, October 25-28, 2001, held in Istanbul, Turkey. See also ADM001351 for entire conference on cd-rom., The original document contains color images.

Abstract

Subject Terms

Report Classification unclassified	**Classification of this page** unclassified
Classification of Abstract unclassified	**Limitation of Abstract** UU

Number of Pages
6

applying the ultrasonic rf-echo phase matching method [3, 4] to the successively acquired rf-echo data frames, or the paired rf-echo data frames, i.e., ones under pre-deformation and post-deformation. In this method, a displacement is determined by using the phase characteristics of the finite local echo data as the index to iteratively search for the corresponding local data. As the change of the local phase characteristics due to tissue deformation deteriorates the accuracy of the determination, the local region size is made suitably smaller during the iterative phase matching. By performing this phase matching throughout the ROI, an accurate displacement vector field data is obtained. The axial/lateral resolutions are respectively determined by the axial/lateral lengths of the final local region. Subsequently, the displacement field data is differentiated using the filter with a cut-off frequency [1] to obtain the strain field data. To determine the globally relative shear modulus distribution with respect to the reference shear moduli, the simultaneous partial differential equations having the strain tensor as the spatially inhomogeneous coefficients are handled. However, as the inevitable strain measurement errors and unfortunate occurred improper configurations of mechanical sources and reference regions make the determination problem ill-conditioned, the robust numerical-based implicit-integration approach [2] is used, which incorporates a computationally efficient regularization method using low-pass filtered spectra derived from strain measurement data. Reconstructed shear modulus distribution is imaged in a log gray scale, in which the bright region indicates that the region is relatively stiff and vice versa.

B. Interstitial RF electromagnetic wave applicator system

The pair of needle electrodes with the diameters of several millimeters are used to apply the electric currents with the frequency of 13.56 MHz. The change of the tissue electric impedance is automatically tracked, and therefore the currents with the power of less than 1 kW can be constantly applied. Using this applicator system and the monitoring technique, the size of the energy-induced thermal lesion can be controlled.

C. In vivo experiment on human breast and liver tissues

The volunteer was 40 years old with papillotubular carcinoma and intraductal papilloma. The size of the carcinoma was larger than papilloma. The volunteer was supinely positioned, and the ROI (43.6 mm x 29.8 mm, spreading from 10.8 mm) was set in her breast tissue. A block reference material of known shear modulus value was put between the ultrasound transducer and her breast, the breast tissue was compressed by the transducer such that the ROI could deform in the scanning plane. The pre-compression and post-compression rf echo data frames were collected. The nominal frequency of the interrogating ultrasound was 7.5 MHz, and the sampling rate was 30 MHz (12 bits). Fig. 1a shows the B-mode image of the ROI under pre-compression. A reference line was set at the depth of 10.8 mm.

The volunteer (male) was healthy 31 years old. The volunteer was supinely positioned, and the ROI (35.7 mm x 49.7 mm, spreading from 35.1 mm) was set in his liver tissue. The tissue was compressed by the ultrasound transducer, and during compression echo data frames were successively acquired. The nominal frequency of the interrogating ultrasound was 8.0 MHz, and the sampling rate was 40 MHz (12 bits). Fig. 2a shows the B-mode image of the ROI, in which a reference line is drawn, i.e., depth of 49.8 mm, where arteries could not be detected. The reference value was set at 1.0.

D. In vitro experiment on calf liver

As shown in the photograph (Fig. 3), the paired needle electrodes were inserted with the angle of 45 degree in parallel into the calf liver specimen. The diameters of the used electrodes were 2 mm, and currents with the power of 100 W were applied.

Specimen 1 (Fig. 4)

The region of the changed ultrasonic reflectivity almost coincided with that in the cutting surface of the visibly detected coagulation. The distance between the needle electrodes was 10 mm. This specimen was mechanically compressed such that the pre-compression and post-compression echo data frames crossed with the paired electrodes could be collected. The nominal frequency of the interrogating ultrasound was 5.0 MHz. In Figs. 4a and 4b, we show the B-mode images of the ROI (the size of 23.3 mm x 19.6 mm, spreading from 2.3 mm) respectively obtained before and after heating under pre-compression. The reference line for shear modulus reconstruction was set at the depth of 2.3 mm, and the reference values were determined by calculating the ratios of the measured strains.

Specimen 2 (Fig. 5)

The spatio-temporal change of shear modulus was monitored. The distance between the needle electrodes was 20 mm. The currents were applied twice for 5 minutes with 10 minutes' interval. Six stages are numbered as follows: (i) before heating, (ii) after 5 minutes' heating, (iii) after 1 minute's leaving, (iv) after more 9 minutes' leaving, (v) after more 5 minutes'

heating, and (vi) after more 10 minutes' leaving. At each stage, the specimen was mechanically compressed such that the echo data frames could be collected in the central plane between the paired electrodes. The nominal frequency of the ultrasound was 8.0 MHz. In Fig. 5a the B-mode images are shown of the ROI (25.1 mm x 39.4 mm, spreading from 3.9 mm) obtained under pre-compression at the stages from (i) to (iv). The reference line was set at the depth of 5.8 mm, and the reference values were determined by calculating the ratios of the measured strains.

Specimen 3 (Fig. 6)

The superficial end of liver had blood vessels with the diameters of about 1 milli-meters, and the region of the ultrasonically detected changes was larger compared with that in the cutting surface of the visibly detected coagulation. The distance between the electrodes was 10 mm. This specimen was compressed such that the echo data frames crossed with the paired electrodes could be collected. The nominal frequency was 5.0 MHz. In Figs. 6a and 6b, the B-mode images are shown of the ROI (the size of 15.0 mm x 17.6 mm, spreading from 4.7 mm) respectively obtained before and after heating under pre-compression. The reference line was set at the depth of 6.0 mm.

Specimen 4 (Fig. 7)

Under the same configurations as that of experiment on specimen 2 the currents were applied twice for 5 minutes with 10 minutes' interval. From B-mode image shown in Fig. 7b after heating, branched blood vessel was visualized of the diameters of about 0.1 mm though it's difficult from the B-mode image in Fig. 7a before heating. The ROI (the size of 23.0 mm x 16.4 mm, spreading from 5.0 mm) was set in parallel in the center of the paired electrodes, the reference line set at the depth of 5.5 mm.

III. RESULTS

A. In vivo experiment of human breast and live tissues

Fig. 1b shows the shear modulus distribution reconstructed on *in vivo* human breast tissue (papillotubular carcinoma case) with the very large dynamic range of 35.8 dB and with the high spatial resolution of 0.8 mm x 3.8 mm. The tumor was estimated to have considerably high shear modulus value, and the estimated highest value of the lesion was 6.33×10^6 N/m^2. The Figs. 1c and 1d shows reconstructions obtained with the smaller regularization parameter values, while Figs. 1e, 1f, and 1g with the spatial resolutions of 1.6 mm x 7.7 mm and with the same regularization parameter values.

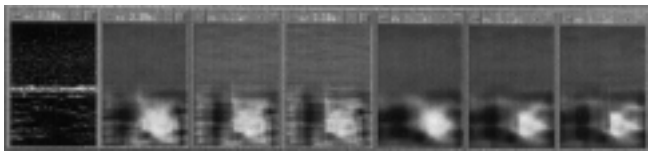

(a) (b) (c) (d) (e) (f) (g)

Fig. 1: *In vivo* human breast tissue (40 years old, ROI size: 43.6 mm x 29.8 mm, depth from 10.8 mm). Images from left to right of B-mode and shear modulus (three images of spatial resolutions of 0.8 mm x 3.8 mm with regularization parameter getting smaller, and three of 1.6 mm x 7.7 mm with the same regularization parameter).

Also on normal *in vivo* human liver tissue the globally relative shear modulus distribution could be stably reconstructed. Fig. 2b shows the reconstruction with the very large dynamic range of 70.2 dB and the high spatial resolution of 4.8 mm x 5.8 mm. As shown, several arteries with the diameters of milli-meter order were estimated to be considerably soft compared with the surrounding tissues.

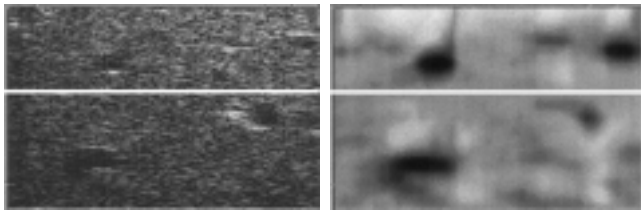

(a) (b)

Fig 2: *In vivo* human liver (31 years old, ROI size: 35.7 mm x 49.7 mm, depth from 35.1 mm to 70.8 mm). Reference line: 49.8 mm. (a) B-mode image and (b) reconstructed relative shear modulus image (dynamic range: 70.2 dB).

B. In vitro experiment on calf liver

Fig. 3: Experimental set up of the *in vitro* calf liver specimen, a pair of the needle electrodes, and the ultrasound transducer.

Specimen 1

In respective Figs. 4a and 4b, the shear modulus images are shown, obtained before and after heating with post 15 minutes' leaving. The dynamic range is 24.1 dB, and the spatial resolution is 1.6 mm x 1.6 mm. It took several ten seconds to

obtain these images (Compaq XP1000, Alpha 500 MHz). Figure. 4c shows the shear modulus image with the dynamic range of 35.1 dB obtained with the smaller regularization parameter value. The photograph (Fig. 4d) of the cutting surface including the ROI show that the elliptic region had gotten higher shear modulus value almost coincided with that of the visibly detected coagulation. Interesting enough, although the Fig. 2d shows laterally unstable reconstruction, we can read in the coagulated region the specific variations of shear modulus value. The instability can be coped with multi-dimensional process [6].

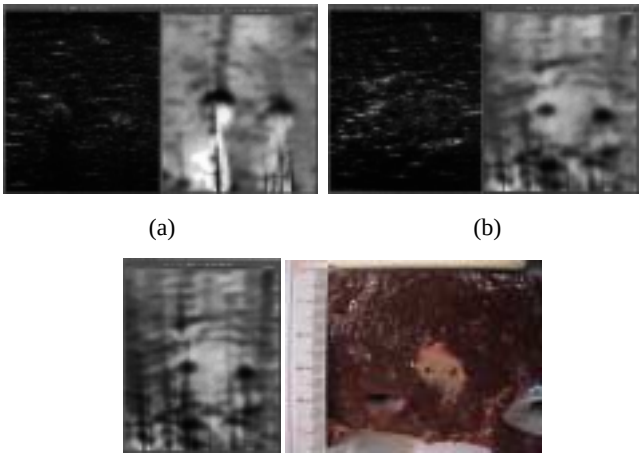

(a) (b)

(c) (d)

Fig. 4. *In vitro* calf liver after applying currents (ROI size of 23.3 mm x 19.6 mm, depth from 2.3 mm). B-mode images (left, pre-compression) and relative shear modulus images (right, DR: 24.1 dB) of (a) before heating, and (b) after heating with post 15 minutes' leaving, (c) shear modulus image obtained with the smaller regularization parameter value (DR: 35.0 dB), (d) photo. of cutting surface including the ROI.

Specimen 2

Fig. 5a shows the shear modulus images obtained at the stages from (i) to (vi). The dynamic range is 79.8 dB, and the spatial resolution is 2.4 mm x 7.2 mm. Although we could not specify the heated region from the series of the B-mode images (stages from (i) to (iv) in Fig. 5a), we could only confirm generation of bubbles due to tissue boiling and fade of the bubbles during cooling down [16, 17]. However, using the series of the shear modulus images we could favorably visualize the spatio-temporal change of tissue elasticity. In order to quantitatively evaluate the change, we show in Fig. 5a the stage versus the mean shear modulus values calculated on the five local regions (8.3 mm x 10.0 mm) depicted in the B-mode image (Fig. 5a－(ii)). We could confirm that the tissue softens by heating (stages (ii) and (v)) and hardens from outside to inside by cooling down ((iii), (iv), and (vi)). By the 1st heating, the mean shear modulus value of the local region 1 (stage (iv)) became about five times higher compared with that of the stage (i). Interestingly enough, the 2nd heating (the stage (vi)) did not allow the mean values at local regions of 1 and 3 to reach the mean values at the 1st heating (iv). The regions might be fragile due to vaporization; then increasing its own plasticity. Finally, the photograph (Fig. 5b) shows the cutting surface including the ROI. The coagulated region detected from the shear modulus image of (iv) well coincided with that of the white region detected in the cutting surface though it's little bit difficult from the shear modulus image of the final stage.

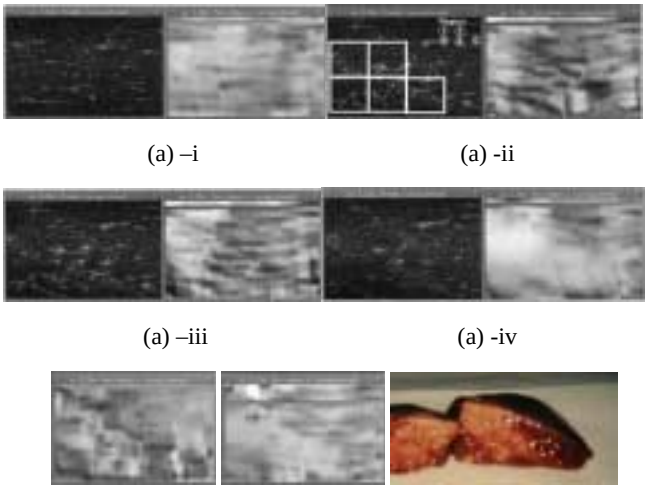

(a) –i (a) -ii

(a) –iii (a) -iv

(a)–iii (a)-iv (b)

(c)

Fig. 5: *In vitro* calf liver (ROI size of 25.1 mm x 39.4 mm, depth from 3.9 mm). (a) B-mode images and relative shear modulus images (dynamic range: 79.8 dB) at five stages: (i) before heating, (ii) after 5 minutes' heating, (iii) after 1 minute's leaving, (iv) after more 9 minutes' leaving, (v) after more 5 minutes' heating, and (vi) after 10 minutes' leaving. (b) Photograph of the cutting surface including ROI. (c) Stages (i) to (vi) vs. the mean relative shear modulus values (5 areas depicted in the B-mode image (a)-ii).

Specimen 3

Figures. 6a and 6b respectively show the shear modulus images obtained before and after heating with post 15 minutes' leaving. The dynamic range is 34.0 dB, and the spatial resolution is 1.6 mm x 1.6 mm. The photograph (Fig. 6c) of the cutting surface including the ROI shows that unexpectedly the lower elliptic tissues and both side blood vessels of the needle-inserted region were coagulated. By digging the coagulated tissues, many blood vessels with the diameters of less 1 mm could be found (Fig. 6d). During cooling down, at the early stage the shear modulus value of the both side blood vessels became higher. However, the shear modulus of the lower region became not so high compared with the side blood vessels. These coagulations are explicitly dependent of the running paths of blood vessels and remaining blood, specifically, the electric resistances and thermal conductivities. As confirmed on other specimens (e.g., Fig. 6e), blood vessels and the surrounding regions got coagulated in early stage compared with other tissues. Thus, the lower region might be shrunk and fragile due to extra induced-thermal energy; then increasing its own plasticity. The large region of ultrasonic changes also seems dependent on the running blood vessels.

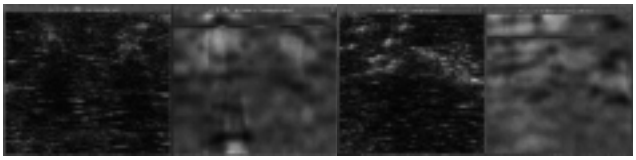

(a) (b)

(c) (d) (e)

Fig. 6: *In vitro* calf liver (ROI size of 15.0 mm x 17.6 mm, depth from 4.7 mm). B-mode (left) and reconstructed relative shear modulus images (right, DR: 34.0 dB): (a) when electrodes inserted before heating, and (b) electrodes ejected after heating with post 15 minutes' leaving. Photos of (c) cutting surface including ROI, (d) coagulated blood vessels, and (e) other specimen.

Specimen 4

The shear modulus value except for the detected blood vessels similarly changed as on specimen 2. Figures. 7a and 7b respectively show the shear modulus images obtained before heating and after heating with post 10 minutes' leaving. The dynamic range is 22.9 dB, and the spatial resolution is 1.6 mm x 1.6 mm. The photograph (Fig. 7c) of the cutting surface including the ROI shows that the region had gotten high shear modulus value almost coincided with that of the visibly detected coagulation. However, though shear modulus value of the blood vessels got high, the value did not reach the value of the surrounding coagulated tissues. As the shear modulus image exhibits the variations in the slice direction, the more quantitative data will be obtained by utilizing 3D reconstruction technique [6].

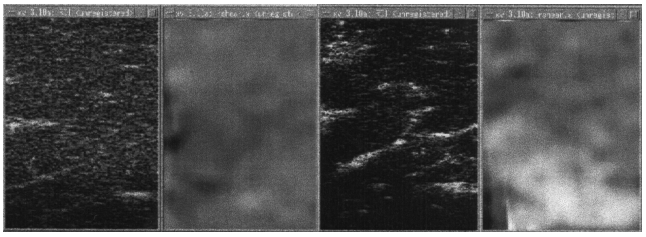

(a) (b)

(c)

Fig. 7. *In vitro* calf liver (ROI size of 23.0 mm x 16.4 mm, depth from 5.0 mm). B-mode (left) and shear modulus images (right, DR: 22.9 dB): (a) before heating, and (b) after heating with 10 minutes' heating. (c) Photo of cutting plane.

Blood vessels with the diameter larger than several millimeters were significantly robust with respect to exposed thermal energy (omitted).

IV. CONCLUSION

Time for shear modulus reconstruction/imaging being dependent on the ROI size, utilization of our developed technique and the conventional Work Station (Compaq XP1000, Alpha 500 MHz) could specify in quasi-real time the tissue elasticity distribution. On the *in vivo* human breast and liver tissues, shear modulus distribution could be stably imaged. In the near future, the limitations for differentiating malignancies of this technique will be reported. Moreover, spatio-temporal change of shear modulus due to heating and cooling down were also shown on the *in vitro* calf liver. Low-invasively obtained various insights about tissue thermal properties will significantly contribute to heightening the effectiveness of various thermal therapies. When performing this kind of the interstitial RF electromagnetic wave thermal therapy, the exposure time should be shorten as much as possible by increasing the output power. Occasionally some cooling device should be also utilized. Ultrasound imaging should

be also conducted. Moreover, together with the temperature monitoring technique [e.g., 18] utilization of our technique will allow HIFU to be widely used. Measured temperature data and reconstructed shear modulus data will be efficiently utilized as the measure for controlling the intension and the foci. This technique can be applied to various treatments. Monitoring and post-treatment data evaluated on *in vivo* human tissues will be also reported. We believe that our technique is currently convenient though 3D reconstruction was in part expected. In the near future these techniques will allow the combined diagnosis/therapy systems to open up a novel clinical style. That is, performing of diagnosis and the subsequently immediate treatment will substantially reduce the total medical expenses. Moreover, the combined systems will be also utilized as screening systems.

ACKNOWLEDGMENT

This research was in part supported by the Japan Society for the Promotion of Science and Technology.

REFERENCES

[1] C. Sumi, A. Suzuki, and K. Nakayama, "Estimation of shear modulus distribution in soft tissue from strain distribution, *IEEE Trans. Biomed. Eng.*, vol. 42, pp. 193－202, 1995.

[2] C. Sumi and K. Nakayama, "A robust numerical solution to reconstruct a globally relative shear modulus distribution from strain measurements," *IEEE Trans. Medical Imag.* Vol. 17, pp. 419－428, 1997.

[3] C. Sumi, A. Suzuki, and K. Nakayama, "Phantom experiment on estimation of shear modulus distribution in soft tissue from ultrasonic measurement of displacement vector field," IEICE Trans.Fundamental, vol. E78-A, pp. 1655－1664, 1995.

[4] C. Sumi, "Fine elasticity imaging utilizing the iterative rf-echo phase matching method," IEEE Trans. Ultrason. Ferroelectr. Freq. Control, vol. 46, pp. 158－166, 1999.

[5] C. Sumi, K. Nakayama, and M. Kubota "An effective ultrasonic strain measurement-based shear modulus reconstruction technique for superficial tissues --- demonstration on *in vitro* pork ribs and in vivo human breast tissues," Phys. Med. Biol., vol. 45, pp. 1511－1520, 2000.

[6] C. Sumi, "Toward 3D reconstruction/imaging shear modulusdistribution in living soft tissues, Proc. of ASJ, pp. 1201-1202, Sep. 1999.

[7] N. T. Wright, S.S. Chen, and J. D. Humphrey, "Time－temperature equivalence of heat-induced changes in cells and proteins," Trans. of ASME, vol. 20, pp. 20－26, 1998.

[8] R. J. Stafford, F. Kallel, R. E. Price, D. M. Cromeens, T. A. Krouskop, J. D. Hazle, and J. Ophir, "Elastographic imaging of thermal lesions in soft tissue: a preliminary study *in vitro*," Ultrasound in Med. & Biol., vol. 24, no. 9, pp. 1449－1458, 1998.

[9] F. Kallel, R. J. Stafford, R. E. Price, R. Righetti, J. Ophir, and J. Hazle, "The feasibility of elastographic visualization of HIFU-induced thermal lesions in soft tissues," Ultrasound in Med. & Biol., vol. 25, no. 4, pp. 641－647, 1999.

[10] R. Righetti, F. Kallel, R. J. Stafford, "Elastographic characterization of HIFU-induced lesions in canine livers," Ultrasound in Med. & Biol., vol. 25, pp. 1099－1113, 1999.

[11] F. Kallel, K. Hirasaki, A. Alaniz, and J. Ophir, "Monitoring low-power heat deposition with elastography," Proc. of 1999 IEEE Ultrasonics Symposium, 1409－1412.

[12] M. M. Doley, J. C. Bamber, I. Rivens, N. L. Bush, and G. R. ter Haar, "Elastographic Imaging of thermally ablated tissue in vivo," Proc. of 1999 IEEE Ultrasonics Symposium, 1631－1634.

[13] C. Sumi, and H. Kanai, "Feasibility of monitoring the thermal therapy by elasticity imaging," Abstracts of the 8th International Congress of Hyperthermic Oncology, p. 191, 2000.

[14] C. Sumi, Y. Ichiki, and H. Kanai, "Feasibility of monitoring thermal therapy by ultrasonic strain measurement-based shear modulus reconstruction," Japanese Journal of Medical Electronics and Biological Engineering, vol. 38, supplement I, p. 284, May 2000 (in Japanese).

[15] C. Sumi, S. Takegahara, and H. Kanai, "Feasibility of shear modulus imaging for monitoring the effectiveness of the interstitial RF electromagnetc wave therapy," Jpn. J. of Hyperthermic Oncol., vol. 16 (suppl.), p. 118, September, 2000 (in Japanese).

[16] C. R. Hill and G. R. Ter Haar, "Review article: High intensity focused ultrasound-potential for cancer treatment," Br. J. Radiol., vol. 68, pp. 1296-1303, 1995.

[17] Watkin NA, G. R.. Ter Haar, S. B. Morris, C. R. J. Woodhouse, "The urological applications of focused ultrasound surgery," Br. J. Urol., vol. 75 (suppl. 1), pp. 1-8, 1995.

[18] R.Seip, and Ebbini, "Non-invasive estimation of tissue/temperature response to heating fields using diagnostic ultrasound," IEEE Trans. Biomed. Eng., vol. 42, pp. 829－839, 1995.